Radiation Physics and Chemistry 115 (2015) 36–42

Contents lists available at ScienceDirect

Radiation Physics and Chemistry

journal homepage: www.elsevier.com/locate/radphyschem

Low energy electrons and swift ion track structure in PADC

Michel Fromm [a,*], Michele A. Quinto [b], Philippe F. Weck [c], Christophe Champion [b]

[a] UMR CNRS 6249 Chrono-Environnement, Université de Bourgogne-Franche-Comté, 16 Route de Gray, F-2530 Besançon Cedex, France
[b] Université de Bordeaux, CNRS/IN2P3, Centre d'Etudes Nucléaires de Bordeaux Gradignan, CENBG, Chemin du Solarium, BP120, 33175 Gradignan, France
[c] Sandia National Laboratories, P.O. Box 5800, MS 0779, Albuquerque, NM 87185, USA

HIGHLIGHTS

- Following-up secondary electron energy cut-offs.
- Energy distribution of Secondary electron distribution of a 100 MeV proton in PADC.
- Sub-ionization electrons and formation of latent track in PADC.

ARTICLE INFO

Article history:
Received 17 December 2014
Received in revised form
2 April 2015
Accepted 4 April 2015
Available online 27 May 2015

ABSTRACT

The current work aims at providing an accurate description of the ion track-structure in poly-allyl dyglycol carbonate (PADC) by using an up-to-date Monte-Carlo code-called TILDA-V (a French acronym for Transport d'Ions Lourds Dans l'Aqua & Vivo). In this simulation the ion track-structure in PADC is mainly described in terms of ejected electrons with a particular attention done to the Low Energy Electrons (LEEs). After a brief reminder of the most important channels through which LEEs are prone to break a chemical bond, we will report on the simulated energetic distributions of LEEs along an ion track in PADC for particular incident energies located on both sides of the Bragg-peak position. Finally, based on the rare data dealing with LEEs interaction with polymers or organic molecules, we will emphasise the role played by the LEEs in the formation of a latent track in PADC, and more particularly the one played by the sub-ionization electrons.

1. Introduction

When ionizing radiation (IR) passes through a medium, due to energy absorption in small volumes, a sequence of very fast reactions along with molecular rearrangements, highly non-homogeneously distributed chemical species such as charged and/or neutral fragments, reactive free radicals and excited chemical intermediates are formed in the medium. The spatial distribution of these arrangements is known as "track structure" (Paretzke, 1987; Magee and Chatterjee, 1987; Kraft and Krämer 1993; Mozumder 1999; LaVerne 2004). Radiation-produced low-energy electrons (LEEs), typically with a kinetic energy lower than 25 eV, are produced in large numbers along an IR track (Bethe, 1933; Pimblott and LaVerne, 2007). Thus, in the early historical developments of quantum mechanical theory for the interaction of radiation with matter, Bethe (Bethe, 1933) showed that during its slowing-down in H_2, a 1 MeV electron produced many secondary electrons among which 77% had kinetic energies lower than 13.54 eV, while at 1 keV, 68.8% of them had energies lower than 13.54 eV. Similarly, Pimblott and LaVerne (Pimblott and LaVerne, 2007) showed that for 1 MeV protons in liquid water, the attenuation of the cascade of secondary electrons and their daughters down to sub-excitation energies (energies lower than the first electronic excitation level of the medium) provided an energy spectrum with about 27% of the electrons having kinetic energies in the range 0–1 eV, the remainder being more or-less equally distributed between 1 and 25 eV. In this case, the mean electron energy of the sub-excitation spectrum was 9 eV. Sub-excitation and sub-ionization electrons can break chemical bonds in particular via dissociative electron attachment (DEA), namely, a resonant process (Schulz, 1973) first discovered in 1930 in gas phase (Lozier, 1930; Schulz, 1959) and more recently in condensed phase (Gallivan and Hamill, 1965; Boudaïffa et al., 2000) and thin films (Lane and Orlando, 2007). The importance of reactions of pre-solvated electrons (LEEs thermalized in water) with biomolecules in aqueous media was pointed out by time-resolved pulse radiolysis experiments in the early seventies (Lenherr and Omerod, 1970). Additionally, LEEs are capable of chemical selectivity (Abdoul-Carime

* Corresponding author.
E-mail address: michel.fromm@univ-fcomte.fr (M. Fromm).

http://dx.doi.org/10.1016/j.radphyschem.2015.04.001
0969-806X/

et al., 2004), contrarily to higher energy electrons. However, since the early development of quantum calculations by Bethe and up to very recent years, secondary electrons have been taken into account in radiation transport Monte Carlo codes only for high kinetic energies, namely, greater than 1–10 keV (see Nikjoo et al. (2006) for a review on the energy cut-off commonly used in the existing Monte Carlo codes). The main reason to use such high-energy thresholds lies in the fact that an accurate description of LEEs transport requires a complete set of multiple and total cross sections, which have remained so far hardly measurable and/or theoretically predictable (Munro et al., 2012). Such operational data only started to be evaluated experimentally over the last two decades for complex systems (Boulanouar et al., 2013). Let us note that specific Monte-Carlo track-structure codes particularly suitable for biophysical modelling at the molecular level exist in the literature with secondary electron energy thresholds of about 10 eV (see for example Champion (2003) and references therein). However, these codes are essentially based on cross-section data for water, the latter being commonly used as surrogate of living matter. In the main, computer codes that are able to describe the behaviour of low energy secondary electrons in any material are very rare and therefore a description of the track-structure taking such LEEs into account only exists for water and some specific components of DNA. In this context, the description of the track-structure of swift ions in PADC will be here provided by using an up-to-date Monte-Carlo code, called TILDA-V, which handles transport of ions in PADC (best known as CR-39™, a widely-used solid state nuclear track detector) for impact energies ranging from 10 keV to 100 MeV and the follow-up of the secondary electrons from 100 keV down to *IP*, the latter referring to the ionization potential of the molecular component of the medium crossed by the radiation.

In this paper, we will present the simulated energetic distributions of ejected LEEs along an ion track in PADC and will point out the role played by the LEEs in the formation of a nuclear track.

2. Proton and electron tracking in PADC

2.1. The TILDA-V Monte Carlo code

The current work aims at providing an accurate description of ion-track in the PADC medium; a polymeric nuclear track detector. To do that, we used the home-made full-differential Monte Carlo (MC) simulation code developed by Champion-called TILDA (a French acronym for Transport d'Ions Lourds Dans l'Aqua)-initially developed for modelling ion and secondary electron histories in liquid and gaseous water for impact energies ranging from 10 keV to 100 MeV/amu (Champion et al., 2005). In a more recent version, TILDA was extended to DNA components with the acronym TILDA-V (the letter V referring to "Vivo"). It is currently based on a complete set of quantum-mechanical/semi-classical cross sections, both multiple differential and integral, able to model all the electron- and proton/hydrogen-induced interactions in water as well as in biological targets, namely the DNA nucleobases and the sugar-phosphate backbone. Under these conditions, TILDA-V represents an event-by-event charged particle transport simulation which consists of a series of random samplings determining successively: (i) the distance travelled by the charged particle between two collisions, (ii) the type of interaction that occurred and finally (iii) the complete kinematics of the resultant particles (the primary-scattered-projectile as well as the potentially created secondary-electron often called δ-ray).

Thus, if the selected interaction is elastic scattering (only for electrons since this process is negligible for heavy projectiles and the trajectory is assumed linear), the corresponding singly differential cross sections are sampled in order to determine the scattering direction, while the electron incident energy E_{inc} remains quasi unchanged, the energy transfer induced during elastic process being very small (of the order of meV). In the case of ionization, the kinetic energy of the ejected electron E_e is first determined by random sampling among the singly differential cross sections, while the ejection and scattering directions are respectively determined from the triply and doubly differential cross sections. The incident particle energy is finally reduced by E_e+IP_j, where IP_j corresponds to the ionization potential of the jth molecular subshell (see hereafter for the PADC description). Finally, if excitation is selected, the relative magnitudes of all the partial excitation cross sections are randomly sampled for selecting an excitation channel n whose corresponding energy E_n is considered as locally deposited. The incident particle energy is then reduced by E_n whereas no angular deflection is assumed, as experimentally observed (Compton and Christophorou, 1967). All these steps are repeated for all primary and secondary particles until their kinetic energy falls below a predetermined cut-off value, here fixed at the ionization potential of the medium. Sub-threshold (sub-ionization) electrons are then assumed to deposit their energy where they are created. In fact, these low-energy species essentially induce vibrational and/or rotational excitations as well as elastic collisions whose total cross section becomes very large, leading to a mean free path of less than 1 nm. Therefore, assuming that these 'killed' particles stay where they have been created introduces uncertainties smaller or of the order of 1 nm in the final energetic cartography.

In the current version of TILDA-V, specially adapted for the study of ion tracking in PADC, we have - in a first attempt-only considered the ionization processes induced by either the ion or the secondary electrons.

The ion-induced ionization process is here described within the semi-empirical and well-documented model called HKS model developed by Hansen, Kocbach and Stolterfoht (Hansen and Kocbach, 1989), which consists in describing the ionization process within the impact parameter 1st Born approximation. In this approach, the initial and the final electron states are described by means of a hydrogenic functions and a plane wave, respectively, *i.e.* without taking into account the electron momentum in its bound state. In this approach, the authors have described the electron emission by heavy ions of charge Z_{ion} in terms of impact parameter dependent probabilities. The doubly differential cross sections, namely, differential in energy transfer and ejection direction, were then obtained by means of analytical integrations of the corresponding probabilities over the impact parameter. However, the original equations proposed by Hansen and Kocbach were recently slightly modified by Bernal and Liendo essentially to avoid the "non-physical" descending jump appearing for each electron binding energy in the singly differential cross sections (Bernal and Liendo, 2006; Bernal and Liendo, 2007). We used this modified model to calculate the doubly and singly differential ionization cross sections (DDCS and SDCS, respectively) induced by ion-impact in PADC. The total ionization cross sections were finally deduced by numerical integration of the SDCS over the ejected energy distribution.

Considering the electron-induced ionization, we have used the semi-empirical model proposed by Kim et al. (Kim and Rudd, 1994), who developed a "binary-encounter-dipole (BED) model", which combines the binary-encounter theory of Vriens (Vriens, 1969) with the dipole interaction of the Bethe theory (Bethe, 1930) for fast incident electrons. The mixing ratios for distant and close collisions, and the interference between the direct and the exchange terms were determined by using the asymptotic behavior predicted by the Bethe theory for ionization and stopping power cross sections. The main inconvenience in the BED model is the

knowledge of the optical oscillator strength data to describe the continuum, which is only available for a limited number of atoms and molecules. However, Kim et al. also proposed an additional approximation in the so-called Binary-Encounter-Bethe (BEB) model where the only needed parameters are: (i) the binding energy, and (ii) the average kinetic orbital energy for all the molecular subshells of the irradiated medium. Besides, relativistic corrections were also taken into account via the relativistic BEB model proposed by Kim et al. (Kim et al., 2000).

2.2. The PADC modelling

The PADC medium is here modelled as an assembly of its monomer ($C_{12}H_{18}O_7$, $M=274.27\ g\ mol^{-1}$)-with a density of $1.32\ g\ cm^{-3}$. The electronic structure calculations were carried out in the gas phase using the Gaussian 09 *ab initio* quantum chemistry software package (Frisch et al., 2009), without symmetry constraints imposed during geometry optimization. The PADC monomer electronic ground state was described using the restricted Hartree–Fock (RHF) method with the 6–311G triple-zeta Gaussian basis sets implemented in Gaussian 09. A number of 73 molecular subshells were then modeled, each of them being populated by 2 electrons. They were then expressed by means of linear combinations of atomic wave functions corresponding to the different atomic components, namely, H_{1s}, C_{1s}, C_{2s}, C_{2p}, O_{1s}, O_{2s} and O_{2p} Clementi-type wave functions. Under these conditions, the electron- and ion-induced ionization cross sections were calculated within the LCAO approach (Linear Combination of Atomic Orbitals), which consists in expressing each "molecular orbital" ionization cross section as a weighted sum of "atomic orbital" cross sections corresponding to the different atomic components involved in the LCAO approach. The latter were then calculated within the corresponding theoretical model, namely, the HKS and the BEB model, respectively, by using the input parameters (binding energy and average kinetic orbital energy; see Table 1 in supplementary material) provided by the 6–311G description of the PADC monomer. Finally, let us note that the theoretical value of 10.31 eV was found for the 1st Ionization Potential (IP) of the PADC monomer.

3. Low energy electrons interaction with matter

As mentioned above, secondary electrons have very low energies, sometimes defined as having a typical energy distribution lying below 70 eV, while the most probable energy is lower than 10 eV

(ICRU, 1979; LaVerne and Pimblott, 1995). At those energies, in the condensed phase, electrons have thermalization distances of the order of 1–10 nm (Cobut et al., 1998), which clearly define the initial volumes for energy/dose deposition of high-energy primary radiations. In such volumes, usually called "spurs," the highly excited atomic, molecular and radical species, ions, and LEEs can induce non-thermal reactions within femtosecond durations (Sanche, 2002). Most of the reactive species, which will initiate chemical reactions, are actually created by the secondary electrons. Thus, based on data for DNA and water targets, Sanche (Sanche, 2002) estimated that about 20% of the energy deposited by fast charged particles in organic matter contributes to the production of electronically excited species that can decay into molecular fragments, whereas the rest leads to ionization. It should be noted that the ionization process releases at least one electron, which in turn will "activate" a spur and so on. Besides, by interacting with another nearby molecule (denoted AB hereafter) and depending on its energy (Sanche, 1995), the secondary electron can either induce further ionization and/or dissociation or temporarily attach to a molecule to form a temporary state AB^{*-} called transient negative ion (TNI). As mentioned by Platzman (Platzman, 1955), LEEs have in a sense a certain transient existence as a unit. In fact, when an incident electron collides with a molecule, the complete list of the different exit pathways is: (1) elastic scattering, (2) inelastic scattering, (3) dissociation into neutrals, (4) dissociation into ground and excited state neutrals, (5) ionization of the parent molecule, (6) dissociation into a neutral and cation, (7) dissociation into an excited state neutral and cation, (8) ion-pair formation, and (9) electron attachment forming a TNI (Ptasinska et al., 2005).

At a microscopic level, electron-molecule collisions are much more complicated than electron-atom collisions due to the additional degrees of freedom that are introduced in the target (vibration and rotation of the nuclei) and in the collision process (dissociation of the molecule into two or more fragments) (Ibănescu, 2009). Electron attachment resonances (TNI) that lead to dissociation are general and prevalent at incident electron energies below 15 eV (Ptasinska et al., 2005). Dissociation also leads to fragments which are often much more reactive than the parent molecules (Ibănescu, 2009). Resonances are characterized by sharp changes in certain scattering cross sections and by transit times that are considerably longer than the normal duration for an electron to pass a molecule (Ibănescu, 2009). We sketch in Fig. 1

Table 1
Energies of electronically excited Feshbach resonances in compounds containing carbonate, ether and alkyl moieties. Shape (vibrational) resonances located at energies lower than 6 eV are not indicated but mentioned in the observation row.

Functional group	Feshbach resonance energy (eV)	Compound	Observation(s)	Ref.
Carbonate		Ethylene carbonate	Numerous shape- and very low-energy resonances identified (<4 eV).	(Stepanović et al., 1999)
	7.5–8		Appearance of fragments with high intensity at low incident electron energies (<4 eV). Loss of α-hydrogen generally due to DEA to carbonyl at low energies.	
Ether (R_1OR_2)	10.5	R_1=methyl	Quasi-independent of R_2	(Ibănescu and Allan, 2009)
Ether (R_1OR_2)	9.1	R_1=ethyl	Quasi-independent of R_2	(Ibănescu and Allan, 2009)
Ether (R_1OR_2)	8.5	R_1=propyl	Quasi-independent of R_2	(Ibănescu and Allan, 2009)
Ether (R_1OR_2)	8.0	R_1=butyl	Quasi-independent of R_2	(Ibănescu and Allan, 2009)
Ether (R_1OR_2)	8.7	R_1=t-butyl	Quasi-independent of R_2	(Ibănescu and Allan, 2009)
Ether (R_1OR_2)	8–9	Linear ethers	Shape resonance at 3.5 eV	(Ibănescu et al., 2008)
Methylene	9–11	Saturated hydrocarbons	Hydrocarbons multilayers. Larger anion fragments (CH^-, CH_2^-, and CH_3^-) produced in much lower abundance.	(Rowntree et al., 1991a, b)

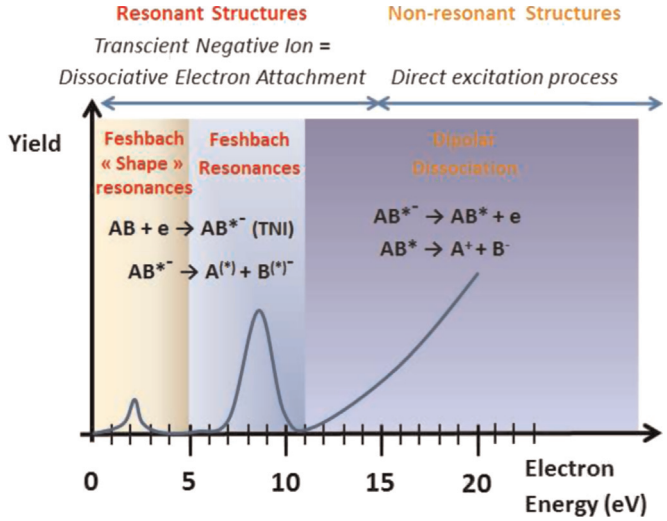

Fig. 1. Cartoon representation of the three energy domains assigned respectively from left to right to shape resonances (typically 0–5 eV), electronically excited Feshbach resonances (typically 5–11 eV) and dipolar dissociation (typically 11 eV up to ionization energy of the considered medium) for organic compounds (Ibănescu and Allan, 2009). All those three energy domains although lying under the ionization potential of the medium can contain processes that lead to molecular dissociation. The two first domains are characterized by specific onsets and resonance energies depending on the considered molecular target. The ordinate-axis is not to scale.

the main structures observed in DEA spectra (via LEEs stimulated desorption of anions, cations or neutrals). Three specific regions are observed: a first one (<5 eV) where the so-called shape resonances (vibrationally excited Feshbach resonances are also observed in this region) are predominant, a second one (5–11 eV) specific to electronically excited Feshbach resonances and a last region (>11 eV), which rises up to the ionization potential of the target where dipolar dissociation (DD) is dominant.

The repeat unit of PADC, is composed of a hydrocarbon chain (methylene groups) through which oxygen atoms are engaged in one ether group and two carbonate ester moieties, the molecule possesses a perfect symmetry with respect to the central ether moiety. Cleavage of the ether bond by LEE impact has recently been studied in the gas phase (Ibănescu et al., 2008) for diethyl ether, dibutyl ether and tetrahydrofuran (THF), the latter being a saturated cyclic molecule. In (Ibănescu et al., 2008), the authors summarized the present knowledge concerning LEE impact on ethers both in the condensed and in the gas phase. In another work of the same group (Stepanović et al., 1999), ethylene carbonate (a saturated cyclic molecule containing the carbonate moiety) and other oxygenated molecules were investigated under LEE impact. More recently, the authors investigated the cleavage of C–O bonds in alcohols and asymmetric ethers (Ibănescu and Allan, 2009). A complete analysis of this work has shown that there was a general rule for many molecules, whereby the lowest resonances (shape resonances) in O-atom containing molecules (i.e., alcohols, ethers, mono-ethers and di-ethers of ethylene glycol, etc) decay by breaking the O–H bond, but not the O–C bond. In contrast, the higher-lying Feshbach resonances, with holes in the σ-orbitals of the alkyl groups, split both the O–H and the O–C bonds. As for the carbonate ester groups of PADC, based on studies involving notably ethylene carbonate, fragment anions were observed at two energy regimes. The higher energy range, $\sim$5–11 eV, was assigned to fragmentation of electronically excited Feshbach resonances. The low-energy range comprises bands below 4 eV, where the number and intensity of the fragments at low energy increase with the number of the oxygen atoms in the molecule. Overall, DEA processes in saturated oxygen-containing compounds are

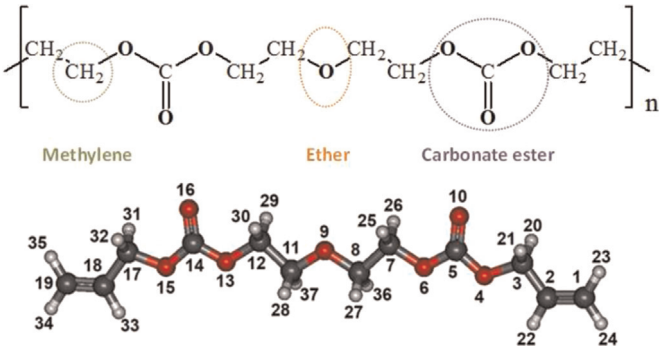

Fig. 2. Chemical structure of the PADC repeat unit. Numbers refer as to the labels used in Table 1 to identify each energy level of the atoms.

mediated by shape resonances, which lead to generally weak fragmentations below 5 eV, and by Feshbach resonances in the 5–11 eV range (Ibănescu and Allan, 2009). Although most of these results are specific to the gas phase, we may anticipate dissociative electron attachment (DEA corresponds to the dissociative decay of a TNI) of ether bonds and in a higher extend of carbonate ester groups in PADC. Above 11 eV, DD also must be observed, as it is a general non-resonant mechanism of molecular dissociation in the low energy domain. We summarize the data of resonance energies (mainly electronically excited Feshbach resonances) gathered in the literature in Table 1 and show the chemical structure of PADC in Fig. 2.

Summarizing the data in Table 1 we may argue that: (i) in saturated hydrocarbons, hydrogen anion elimination is by far the dominant DEA mechanism (Rowntree et al., 1991a), (ii) in addition to the Feshbach resonance around 7.5–8 eV (*i.e.* many different fragments for these "high energy" processes), the carbonate group is subject to numerous vibrational or shape resonances at low energy (<5 eV) (Stepanović et al., 1999), (iii) ether groups dissociate mainly through Feshbach resonance near to 8–9 eV (Ibănescu and Allan, 2009). The CO bond is cleaved also by 3.5 eV electrons in the linear ethers (Ibănescu et al., 2008). It should be noted that, except in the case of saturated hydrocarbons, all other compounds were analyzed in the gas phase; fragmentation patterns in the condensed phase might be somewhat different from the gas phase. Also important is the fact that resonance energies are not equal to the onsets for DEA; those latter values are generally at least of 2–3 eV lower than the resonance energy depending on the width of the resonance band.

4. Low energy electrons and track structure in PADC

A first TILDA-V simulation aiming at computing the energy distributions of ejected secondary electrons due to the slowdown of a proton in PADC was performed. Ejected electron energies were computed far away and on both sides of the Bragg-peak and expressed under the form of statistical distributions for initial proton energies of 100 MeV, 10 MeV, 1 MeV, 100 keV and 12 keV. These results are presented in Fig. 3. It appears that the mean ejected electron energy, which characterizes a given distribution, depends on the initial energy of the proton and therefore may be seen as depending also on LET. More interesting is the fact that for almost similar proton LET values (corresponding to kinetic energies of 10 MeV and 12 keV, *i.e.* situated on both sides of the Bragg-peak), the mean energies of the secondary electron distributions differ notably, namely, 54.4 eV and 8.1 eV, respectively.

In a general way, the mean ejected electron energies that characterize each of the computed distributions appear lower as

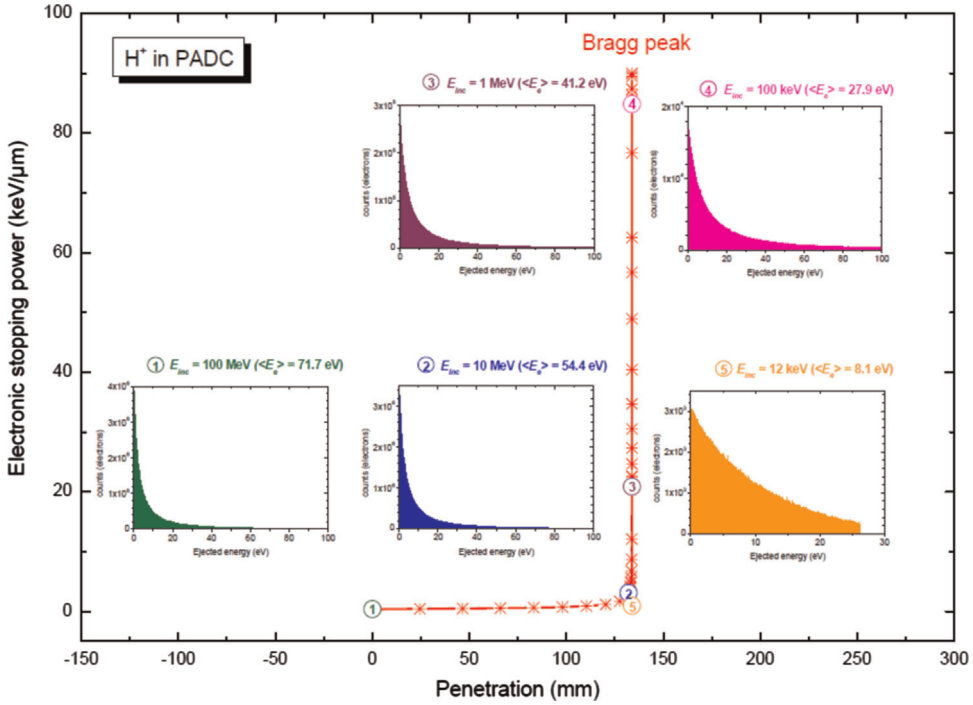

Fig. 3. Bragg-peak for 100 MeV proton in PADC material as computed by the TILDA-V software (red line). Ejected electron energies computed far away and on both sides of the Bragg-peak are also reported for initial proton energies of 100 MeV, 10 MeV, 1 MeV, 100 keV and 12 keV. They are here expressed under the form of statistical distributions. For each of them, the mean secondary electron energy (Expected value) is reported over the respective energy-distribution plot. (For interpretation of the references to color in this figure legend, the reader is referred to the web version of this article.)

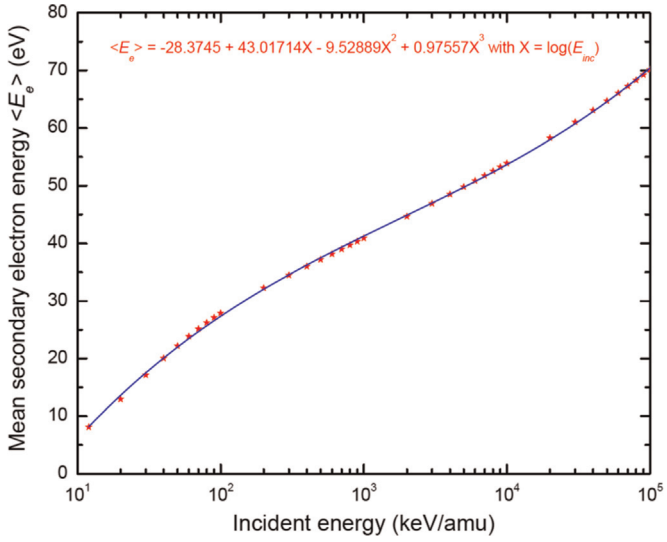

Fig. 4. Mean ejected electron energies (expressed in eV) along the trajectory of a projectile in PADC plotted versus the kinetic projectile energy E_{inc} (expressed in keV/amu). The red stars indicate the Monte Carlo results while the dotted blue line refers to the polynomial fit whose expression is reported on the plot. (For interpretation of the references to color in this figure legend, the reader is referred to the web version of this article.)

may be anticipated from basic physics concepts. It is indeed usual to estimate the maximum secondary electron energy (kinematic limit E_e^{max}) based on a simple knock-on classical mechanics collision formula (interaction with a single atomic electron treated as free and at rest, usually seen as an elastic scattering of two hard spheres) with a moving proton with initial kinetic energy E_{inc}:

$$E_e^{max} = \left(\frac{4m_0}{M_p}\right)E_{inc} \quad (1)$$

where the ratio of the electron mass (m_0) over the proton mass (M_p) is of the order of 1/1836.

Thus, Eq.(1) yields for instance a maximum secondary electrons energy of about 220 keV, 20 keV, 2 keV, 220 eV and 26 eV for initial proton energies of 100 MeV, 10 MeV, 1 MeV, 100 keV and 12 keV, respectively; the three first electron energies being relativistic. But, when comparing the mean energies computed by means of Monte Carlo method (TILDA-V) it clearly appears that the most-probable energies are systematically lower than 100 eV, *i.e.* tending to the domain of the so-called Low Energy Electrons. At the maximum of the stopping power (protons with 100 keV, *i.e.* at the Bragg-peak), the mean ejection energy of the secondary electrons is 27.9 eV. For the highest initial proton energy, namely, E_{inc}=100 MeV, interaction with PADC is characterized by a mean electron ejection energy of 71.7 eV.

Comparatively, the Stopping and Range of Ions in Matter code provides corrected values for the mean ionization potential ($\langle I\rangle$) for protons and helium ions slowed in elemental targets (Ziegler, 2008):

$\langle I\rangle$=79.1 eV for carbon, $\langle I\rangle$=96.0 eV for oxygen, their first IPs being respectively 11.26 and 13.62 eV. Thus, it is clear that a noticeable fraction of all the secondary electrons produced by a 100 MeV proton, from its entry in the PADC target to the thermalization point, has such or even lower initial energies (*i.e.* at the moment of their ejection) than the elemental mean IPs of the atomic constituents and should therefore be ignored if only ionization would be taken into account.

This shows the absolute necessity of taking into account all the processes and not limiting the electron-induced collisions to the excitation and the ionization processes, in particular by counting the DEA process, which is highly damaging at sub-ionization energies.

In order to generalize our purpose, mean energies of electron ejected in PADC have also been calculated as a function of the incident projectile kinetic energy ranging from 10 up to 10^5 keV/amu. Let us note that the current calculations are carried

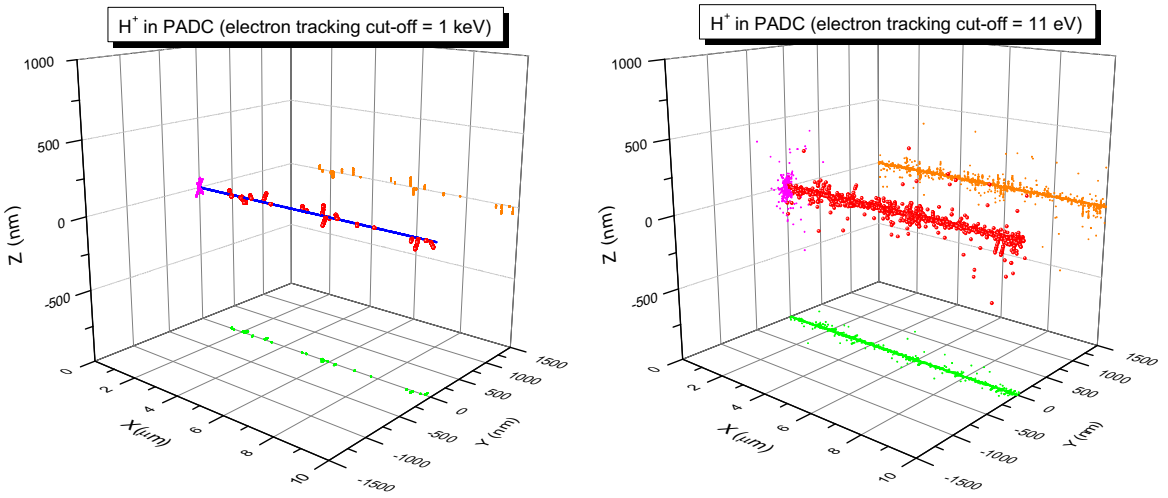

Fig. 5. 3D-plot of a 10 μm track for a 1 MeV proton in PADC. The energy cut-off for the secondary electron following-up is successively fixed at 1 keV (left) and 11 eV (right). In both cases, the blue circles represent the proton interactions, whereas the red ones represent the secondary electron induced collisions. Orange, magenta and green points refer to the *XZ*-, *YZ*- and *XY*-plane projections, respectively. (For interpretation of the references to color in this figure legend, the reader is referred to the web version of this article.)

out at the 1st Born (*perturbative*) approximation, which implies that the obtained values of mean ejected electron energy are independent of the projectile, since in the *perturbative* framework the singly differential cross sections, namely, differential in the ejected energy, are proportional to the square of the projectile charge and then lead to a mean ejected electron energy independent of the charge of the incident ion. Thus, once plotted versus the incident projectile energy-expressed in keV/amu-these data may be seen as a "universal plot" (see Fig. 4).

Fig. 4 shows that any non-relativistic swift ion liberates secondary electrons along its track with a mean energy that remains lower than 70 eV. Such sub-ionization electrons will for a significant part, fall in the range of the so-called LEE's (typically 0–25 eV) after very few inelastic scattering(s) if they will not cause dipolar dissociation.

In order to illustrate the important role of the cut-off energy set in track-structure simulation codes, a three-dimensional representation of a 10 μm-track for a 1 MeV proton in PADC is depicted in Fig. 5 for 2 different values of electron tracking cut-off, namely, 1 keV and 11 eV.

Fig. 5 illustrates the dramatic change observed in quantifying ejected secondary electrons along the projectile's trail with dependence of the energy cut-off, notably in terms of number of secondary electrons and their energy distribution. This comparison emphasizes the importance of energy cut-offs used in MC codes but also demonstrate the considerable number of harmful LEEs produced in an ion track.

5. Discussion and conclusion

Using cut-off energy of 10.31 eV (fixed at the first ionization potential of the PADC monomer as computed using the GAUSSIAN calculation software), the TILDA-V MC simulations presented herein have shown that LEEs constitute an abundant fraction of the total number of ejected secondary electrons along a proton track. Performed for the first time on PADC material, such refined calculations show not only the fact that average initial secondary electron energies are rather small compared to the kinematic limit of secondary electrons (see Eq.(1)), but also that those mean energies which are specific to the incident ion energy are different for two same LET values collected on both sides of the Bragg peak. It is especially particularly interesting to note that 10 MeV and 12 keV protons slowed down in PADC with quasi-identical LETs have average ejection energies of their secondary electron distributions of respectively 54.4 eV and 8.1 eV, the latter lying under the theoretical value of the first IP of PADC. Such differences in the mean energy of the distributions of ejected secondary electrons for a same LET value may constitute a fundamental answer to the observation made of extremely important differences in the specific track-etch rates measured on both sides of the Bragg-peak (Fromm et al., 2004) most probably due to the fact that LEEs are capable of chemical selectivity (Ibănescu and Allan, 2009). Based on a bibliographical survey, we have shown (see Section 3) that LEEs are likely to damage the molecular constituents of PADC even at energies lower than the material's first IP by means of DEA and possibly DD processes. In the absence of experimental and/or theoretical cross sections describing these processes or at least onset values for the formation of TNIs in PADC, we can only speculate on the exact role of LEEs in the formation of a nuclear track. Nevertheless, data exist on the radiation chemistry of PADC which can help us understand how LEEs could participate in the physicochemistry of the track-structure. The work by Yamauchi, Barillon and co-workers exploiting proton and heavy ion PADC irradiations in a wide range of stopping powers is especially relevant to this aim. In a recent paper of this team compiling data obtained using various ions at different energies (Mori et al., 2011), it is shown that over all the projectiles studied, the highest G-values was observed in the films irradiated with 5.7 MeV protons; i.e. about 20 scissions/100 eV for both bonds (ether and carbonate ester) with LET=9 keV/μm. As can be seen in Fig. 3, the maximum G-values which concern 5.7 MeV protons are located in the Bragg-peak region and must then be characterized by mean ejected secondary electron energies ranging between 41.2 and 54.4 eV.

If this observation is in favor of a noticeable contribution of LEEs in the formation of a nuclear track in PADC, it does not constitute a complete proof and further studies will have to provide more details. With this objective in mind, we are currently working on fabricating ultra-thin PADC foils (typically nanometer-scaled) in order to study their electron stimulated desorption spectra which might reveal the type and nature of molecular fragments produced under LEE impact as well as the onsets and resonance energies which characterize the formation of these molecular fragments.

Acknowledgments

This work was partially supported by the "INSERM PCPHY MICRONAUTE (2013-2014)" project. Sandia National Laboratories is a multiprogram laboratory operated by Sandia Corporation, a wholly owned subsidiary of Lockheed Martin Company, for the United States Department of Energy's National Nuclear Security Administration under Contract DE-AC04-94AL85000.

Appendix A. Supplementary material

Supplementary data associated with this article can be found in the online version at http://dx.doi.org/10.1016/j.radphyschem.2015.04.001.

References

Abdoul-Carime, H., Gohlke, S., Illenberger, E., 2004. Phys. Rev. Lett 92, 168103.
Bernal, M.A., Liendo, J.A., 2006. The HKS model for electron production in liquid water by light ions. Nucl. Instrum. Methods Phys. Res. Sect. B 251, 171–176.
Bernal, M.A., Liendo, J.A., 2007. Inelastic-collision cross sections for the interactions of totally stripped H, He and C ions with liquid water. Nucl. Instrum. Methods Phys. Res. Sect. B 262, 1–6.
Bethe, H., 1930. Zur Theorie des Durchgangs schneller Korpuskularstrahlen durch Materie. Ann. Phys. 5, 325.
Bethe, H.A., 1933. (V) Quantenmechanik der Ein- und Zweielectronenprobleme. Handbuch der Physik. 24. Springer, Berlin.
Boudaïffa, B., Cloutier, P., Hunting, D., Huels, M.A., Sanche, L., 2000. Resonant formation of DNA strand breaks by low-energy (3–20 eV) electrons. Science 287 (5458), 1658–1660.
Boulanouar, O., Fromm, M., Bass, A.D., Cloutier, P., Sanche, L., 2013. Absolute cross section for loss of supercoiled topology induced by 10 eV electrons in highly uniform/DNA/1,3-diaminopropane films deposited on highly ordered pyrolitic graphite. J. Chem. Phys. 139 (5), 055104–055104-7.
Champion, C., 2003. Theoretical cross sections for electron collisions in water: structure of electron tracks. Phys. Med. Biol. 48, 2147–2168.
Champion, C., L'Hoir, A., Politis, M.-F., Fainstein, P.D., Rivarola, R.D., Chetioui, A., 2005. A Monte Carlo code for the simulation of heavy-ion tracks in water. Radiat. Res. 163, 222–231.
Cobut, V., Frongillo, Y., Patau, J.P., Goulet, T., Fraser, M.-J., Jay-Gerin, J.-P., 1998. Monte Carlo simulation of fast electron and proton tracks in liquid water-I. Physical and physicochemical aspects. Radiat. Phys. Chem. 51, 229–243.
Compton, R.N., Christophorou, L.G., 1967. Negative-ion formation in H_2O and D_2O. Phys. Rev. 154, 110.
Frisch, M.J., et al., 2009. *Gaussian 09*, Revision A.02. Gaussian, Inc., Wallingford CT.
Fromm, M., Awad, E.M., Ditlov, V., 2004. Many-hit model calculations for track etch rate in CR-39 SSNTD using confocal microscope data. Nucl. Instrum. Methods Phys. Res. B 226, 565–574.
Gallivan, J.B., Hamill, W.H., 1965. Evidence for dissociative electron attachment in γ-irradiated hydrocarbon glasses. Trans. Faraday Soc. 61, 1960–1967.
Hansen, J.P., Kocbach, L., 1989. Ejection angles of fast delta electrons from K-shell ionization induced by energetic ions. J. Phys. B 22, 71–78.
Ibănescu, B.C., May, O., Allan, M., 2008. Cleavage of the ether bond by electron impact: differences between linear ethers and tetrahydrofuran. Phys. Chem. Chem. Phys. 10, 1507–1511.
Ibănescu, B.C., 2009. Electron-driven chemistry of saturated compounds containing oxygen or nitrogen atoms. (Ph.D. thesis). University of Fribourg, Switzerland, p. 1628.
Ibănescu, B.C., Allan, M., 2009. Selective cleavage of the C–O bonds in alcohols and asymmetric ethers by dissociative electron attachment. Phys. Chem. Chem. Phys. 11, 7640–7648.
International Commission on Radiation Units and Measurements, 1979. ICRU Report 31. ICRU, Washington DC.
Kim, Y. –K., Rudd, M.E., 1994. Binary-encounter-dipole model for electron-impact ionization. Phys. Rev. A 50, 3954.
Kim, Y.-K., Santos, J.P., Parente, F., 2000. Extension of the binary-encounter-dipole model to relativistic incident electrons. Phys. Rev. A 62, 052710.
Kraft, G., Krämer, M., 1993. Linear energy transfer and track structure. Adv. Radiat. Biol. 17, 1–52.
LaVerne, J.A., Pimblott, S.M., 1995. Electron energy-loss distributions in solid, dry DNA. Radiat. Res. 141, 208–215.
LaVerne, J.A., 2004. Radiation chemical effects of heavy ions. In: Mozumder, A., Hatano, Y. (Eds.), Charged Particle and Photon Interactions with Matter. Chemical, Physicochemical, and Biological Consequences with Application. Marcel Dekker, New York, pp. 403–429.
Lane, C.D., Orlando, T.M., 2007. Inelastic electron scattering and energy-selective negative ion reactions in molecular films on silicon surfaces. Appl. Surf. Sci. 253, 6646–6656.
Lenherr, A.D., Omerod, M.G., 1970. Electron reactions in γ-irradiated thymidine and cystamine. Nature 225, 546.
Lozier, W.W., 1930. Negative ions in hydrogen and water vapor. Phys. Rev. 36, 1417.
Magee, J.L., Chatterjee, A., 1987. Track reactions of radiation chemistry. In: Freeman, G.R. (Ed.), Kinetics of Nonhomogeneous Processes. Wiley, New York, pp. 171–214.
Mori, Y., Yamauchi, T., Kanasaki, M., Maeda, M., Oda, Y., Kodaira, K., Konishi, S., N., T., Yasuda, N., Barillon, R., 2011. Radiation chemical yields for loss of ether and carbonate ester bonds in PADC films exposed to proton and heavy ion beams. Radiat. Meas. 46, 1147–1153.
Mozumder, A., 1999. Fundamentals of Radiation Chemistry. Academic Press, San Diego, California.
Munro, J.J., Harrison, S., Fujimoto, M.M., Tennyson, J., 2012. A dissociative electron attachment cross-section estimator. J. Phys.: Conf. Ser. 388, 012013.
Nikjoo, H., Uehara, S., Emfietzoglou, D., Cucinotta, F.A., 2006. Track-structure codes in radiation research. Radiat. Meas. 41, 1052–1074.
Paretzke, H.G., 1987. Radiation track structure theory. In: Freeman, G.R. (Ed.), Kinetics of Nonhomogeneous Processes. Wiley, New York, pp. 89–170.
Pimblott, S.M., LaVerne, J.A., 2007. Production of low-energy electrons by ionizing radiation. Radiat. Phys. Chem. 76, 1244.
Platzman, R.L., 1955. Subexcitation electrons. Radiat. Res. 2, 1–7.
Ptasinska, S., Denifl, S., Scheier, P., Illenberger, E., Märk, T.D., 2005. Bond- and site-selective loss of H atoms from nucleobases by very-low-energy electrons (<3 eV). Angew. Chem. Int. 42 (44), 6941–6943.
Rowntree, P., Parentau, L., Sanche, L., 1991a. Anion yields produced by low-energy electron impact on condensed hydrocarbon films. J. Phys. Chem. 95, 4902–4909.
Rowntree, P., Parenteau, L., Sanche, L., 1991b. Dielectric Polarization Invariance In Dissociative Electron Attachment from Condensed Saturated Hydrocarbons. J. Phys. Chem 95, 523–524.
Rowntree, P., Parenteau, L., Sanche, L., Sanche, L., 1995. Interaction of low-energy electrons with atomic and molecular solids. Scanning Microsc. 9, 619–656.
Sanche, L., 2002. Nanoscopic aspects of radiobiological damage: fragmentation induced by secondary low-energy electrons. Mass Spectrom. Rev. 21 (5), 349–369.
Schulz, G.J., 1959. Formation of H^- ions by electron impact on H_2. Phys. Rev. 113, 816.
Schulz, G.J., 1973. Resonances in electron impact on diatomic molecules. Rev. Mod. Phys. 45 (3), 423–486.
Stepanović, M., Pariat, Y., Allan, M., 1999. Dissociative electron attachment in cyclopentanone, γ-butyrolactone, ethylene carbonate, and ethylene carbonate-d4: role of dipole-bound resonances. J. Chem. Phys. 110 (23), 11376.
Vriens, L., 1969. In: McDaniel, E.W., McDowell, M.R.C. (Eds.), Case Studies in Atomic Physics, 1. North-Holland, Amsterdam, p. 335.
Ziegler, J. F., 2008. SRIM – The Stopping power and Range of Ions in Matter. ⟨http://www.srim.org/SRIM/SRIMPICS/IONIZ.htm⟩.